

Spinodal instabilities and the distillation effect in nuclear matter under strong magnetic fields.

A. Rabhi,^{1,2,*} C. Providência,^{1,†} and J. Da Providência^{1,‡}

¹*Centro de Física Teórica, Department of Physics,
University of Coimbra, 3004-516 Coimbra, Portugal*

²*Laboratoire de Physique de la Matière Condensée,
Faculté des Sciences de Tunis, Campus Universitaire, Le Belvédère-1060, Tunisia*

(Dated: October 30, 2018)

We study the effect of strong magnetic fields, of the order of $10^{18} - 10^{19}$ G, on the instability region of nuclear matter at subsaturation densities. Relativistic nuclear models both with constant couplings and with density dependent parameters are considered. It is shown that a strong magnetic field can have large effects on the instability regions giving rise to bands of instability and wider unstable regions. As a consequence we predict larger transition densities at the inner edge of the crust of compact stars with strong magnetic field. The direction of instability gives rise to a very strong distillation effect if the last Landau level is only partially filled. However, for almost completed Landau levels an anti-distillation effect may occur.

PACS numbers: 21.65.-f 26.60.Kp 26.60.-c 97.60.Jd

I. INTRODUCTION

Recent investigations seem to show that soft γ -ray repeaters and some anomalous X-ray pulsars are neutron stars which may have surface magnetic fields larger than 10^{15} G [1–3], the so called magnetars. Until recently, the strongest estimated magnetic field is of the order of $B = 2 \times 10^{15}$ G and was detected in a quite young star, SGR 1806-20 [4]. According to [5] a fraction as high as 10% of the neutron star population could be magnetars.

The effect of the strong magnetic fields on the equation of state (EOS) of stellar matter in neutron stars has been studied both at low densities below neutron drip, of interest for the study of the outer crust of neutron stars [6], and at high densities, of interest for the study of the interior of compact stars [7, 8]. In this last case field-theoretical descriptions based on the non-linear Walecka model (NLWM) [9] were used and several parametrizations compared. It was shown that they have an overall similar behavior. It was recently shown in [10] that the EOS at subsaturation densities, including densities of the order of the densities at the inner edge of the crust of a compact star, was particularly affected by fields of the order of 10^{18} G.

An important characteristic of the nuclear matter is the appearance of a liquid-gas phase transition at subsaturation densities. The role of the isospin is of particular importance. Indeed, since nuclear matter is composed of two different fluids, namely protons and neutrons, the liquid-gas phase transition can lead to an isospin distillation phenomenon [11]. The region of instability is determined by the spinodal curve. Due to the symmetry energy, the EOS of β -equilibrium of magnetic free nuclear matter is thermodynamically stable. The stability of the EOS is determined from the curvature of the free-energy: a positive curvature corresponds to thermodynamically stable matter.

If we consider stellar matter at very low densities, nuclei in matter are expected to form a Coulomb lattice embedded in the neutron-electron sea that minimizes the Coulomb interaction energy. With an increase of the density, nuclear "pasta" structures emerge [12]. The existence of pasta phases may modify some important processes by changing the hydrodynamic properties and the neutrino opacity in supernova matter and in the matter of newly born neutron stars [13]. Also, the pasta phases may influence neutron star quakes and pulsar glitches via the change of mechanical properties of the crust matter [14]. It is therefore important to study how the magnetic field could affect the extension of the pasta phase and the isospin distillation effect.

In fact, sufficiently strong magnetic field affect the extension of the unstable region. In order to have a better understanding of the effect of the magnetic field on the instabilities of nuclear matter at subsaturation densities we study in the present work the effect of a strong magnetic field on the thermodynamical spinodal instabilities obtained from the free energy curvature matrix [15, 16]. Recently, it was shown that the magnetic field and Joule heating have

*Electronic address: rabhi@teor.fis.uc.pt

†Electronic address: cp@teor.fis.uc.pt

‡Electronic address: providencia@teor.fis.uc.pt

the important effect of maintaining compact stars warm for a longer time [17]. This kind of simulations need the EOS of the crust. It is, therefore, important to make a study that shows when should the magnetic field be taken explicitly into account in the EOS of the crust. An unstable region in a wider density range will correspond to a larger crust and the properties of the star depending on the crust will be affected.

In the present paper, we will consider two relativistic effective approaches: a NLWM, TM1 [18], with constant coupling parameters, and a density dependent relativistic hadronic (DDRH) model TW [19] with density-dependent coupling parameters. DDRH models seem to give results closer Skyrme interactions than NLWM, at subsaturation densities [20].

In section II we make a brief review of the models, the EOS under the effect of a magnetic field and the stability conditions. Results are discussed in section III and conclusions are drawn in the last section.

II. THE FORMALISM

A. EOS of nuclear matter under a strong magnetic field

In the present section we make a short review of the field-theoretical approach used to obtain the EOS of nuclear matter. Within this approach, the baryons interact via the exchange of σ , ω and ρ mesons in the presence of a uniform magnetic field B along the z -axis. We start from the Lagrangian density of TW [19, 21] model

$$\mathcal{L} = \sum_{b=n,p} \mathcal{L}_b + \mathcal{L}_m. \quad (1)$$

The baryon ($b=n, p$) and meson (σ, ω and ρ) Lagrangians are given by

$$\begin{aligned} \mathcal{L}_b &= \bar{\Psi}_b \left(i\gamma_\mu \partial^\mu - q_b \gamma_\mu A^\mu - m_b + \Gamma_\sigma \sigma - \Gamma_\omega \gamma_\mu \omega^\mu - \frac{1}{2} \Gamma_\rho \tau_{3b} \gamma_\mu \rho^\mu - \frac{1}{2} \mu_N \kappa_b \sigma_{\mu\nu} F^{\mu\nu} \right) \Psi_b, \\ \mathcal{L}_m &= \frac{1}{2} \partial_\mu \sigma \partial^\mu \sigma - \frac{1}{2} m_\sigma^2 \sigma^2 + \frac{1}{2} m_\omega^2 \omega_\mu \omega^\mu - \frac{1}{4} \Omega^{\mu\nu} \Omega_{\mu\nu} \\ &\quad - \frac{1}{4} F^{\mu\nu} F_{\mu\nu} + \frac{1}{2} m_\rho^2 \rho_\mu \rho^\mu - \frac{1}{4} P^{\mu\nu} P_{\mu\nu}, \end{aligned} \quad (2)$$

respectively, where Ψ_b are the baryon Dirac fields. The nucleon mass and isospin projection for the protons and neutrons are denoted by m_b and $\tau_{3b} = \pm 1$, respectively. The mesonic and electromagnetic field strength tensors are given by their usual expressions: $\Omega_{\mu\nu} = \partial_\mu \omega_\nu - \partial_\nu \omega_\mu$, $P_{\mu\nu} = \partial_\mu \rho_\nu - \partial_\nu \rho_\mu$, and $F_{\mu\nu} = \partial_\mu A_\nu - \partial_\nu A_\mu$. The nucleon anomalous magnetic moments are introduced via the coupling of the baryons to the electromagnetic field tensor with $\sigma_{\mu\nu} = \frac{i}{2} [\gamma_\mu, \gamma_\nu]$ and strength κ_b with $\kappa_n = g_n/2 = -1.91315$ for the neutron and $\kappa_p = (g_p/2 - 1) = 1.79285$ for the proton, respectively, and where g_i are the Landé g factors for the particle i ($g_p = 5.5856912$ and $g_n = -3.8260837$), and μ_N is the nuclear magneton. The electromagnetic field is assumed to be externally generated (and thus has no associated field equation), and only frozen-field configurations will be considered. The electromagnetic couplings are denoted by q . The parameters of the model are the nucleon mass $m_b = 939$ MeV, the masses of mesons m_σ , m_ω and m_ρ and the density dependent coupling parameters Γ which are adjusted in order to reproduce some of the nuclear matter bulk properties and DBHF (Dirac Brueckner Hartree-Fock) calculations [22], using the following parametrization

$$\Gamma_i(\rho) = \Gamma_i(\rho_{sat}) f_i(x), \quad i = \sigma, \omega, \rho \quad (3)$$

where $x = \rho/\rho_{sat}$, with

$$f_i(x) = a_i \frac{1 + b_i (x + d_i)^2}{1 + c_i (x + d_i)^2}, \quad i = \sigma, \omega, \quad (4)$$

and,

$$f_\rho(x) = \exp[-a_\rho(x - 1)], \quad (5)$$

with the values of the parameters m_i , Γ_i , a_i , b_i , c_i and d_i , $i = \sigma, \omega, \rho$ given in Table I for TW model [19]. Other possibilities for these parameters are also found in the literature [23].

i	$m_i(\text{MeV})$	Γ_i	a_i	b_i	c_i	d_i
σ	550	10.72854	1.365469	0.226061	0.409704	0.901995
ω	783	13.29015	1.402488	0.172577	0.344293	0.983955
ρ	763	7.32196	0.515			

TABLE I: Parameters of the TW model.

The symmetry energy and its first and second derivatives are important to understand the instability region. NLWM models become very stiff above saturation densities while DDRH models have a softer behavior. On the other hand, at subsaturation densities DDRH models have larger symmetry energies and a larger extension of the instability region for very asymmetric matter. In Fig. 1 we compare the symmetry energy of the models we will consider in the present study: TM1 and TW. As expected TM1 has a smaller symmetry energy at subsaturation densities and a larger one above the saturation density.

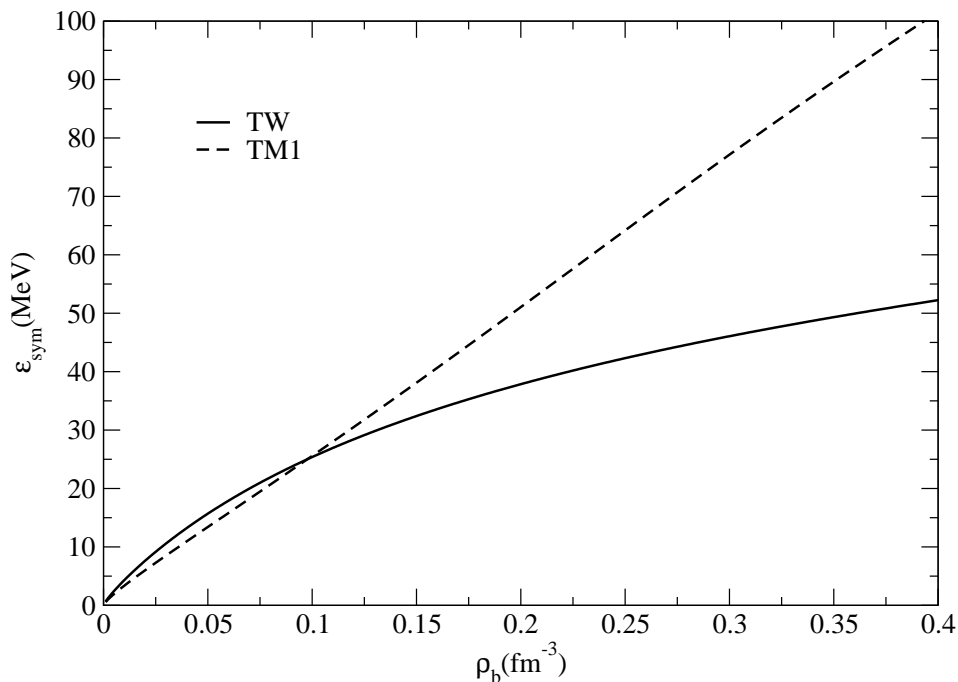


FIG. 1: Symmetry energy for all models used in the present work.

Notice that in the DDRHM the nonlinear meson terms are not present, in contrast with the usual NLWM. For TM1 model we add to the Langrangian density, Eq. (21), with $g_i = \Gamma_i$,

$$\mathcal{L} = \frac{1}{3}bm_n(g_\sigma\sigma)^3 + \frac{1}{4}c(g_\sigma\sigma)^4 + \frac{1}{4!}\xi g_\omega^4(\omega_\mu\omega^\mu)^2.$$

The coupling parameters are constant and given in [18].

From now we take the standard mean-field theory (MFT) approach and display only some of the equations. A complete set of equations and description of the method can be found in the literature (*e.g.*, Ref. [7, 24]). For the description of the system, we need the baryonic density, the energy density of nuclear matter, and the pressure. The energy density of nuclear matter is given by

$$\varepsilon = \sum_{b=p,n} \varepsilon_b + \frac{1}{2}m_\sigma^2\sigma^2 + \frac{1}{2}m_\omega^2\omega_0^2 + \frac{1}{2}m_\rho^2\rho_0^2 \quad (6)$$

where the energy densities of nucleons have the following forms

$$\begin{aligned}\varepsilon_p &= \frac{q_p B}{4\pi^2} \sum_{\nu,s} \left[k_{F,\nu,s}^p E_F^p + \left(\sqrt{m^{*2} + 2\nu q_p B} - s\mu_N \kappa_p B \right)^2 \ln \left| \frac{k_{F,\nu,s}^p + E_F^p}{\sqrt{m^{*2} + 2\nu q_p B} - s\mu_N \kappa_p B} \right| \right], \\ \varepsilon_n &= \frac{1}{4\pi^2} \sum_s \left[\frac{1}{2} k_{F,s}^n E_F^{n3} - \frac{2}{3} s\mu_N \kappa_n B E_F^{n3} \left(\arcsin \left(\frac{\bar{m}_n}{E_F^n} \right) - \frac{\pi}{2} \right) - \left(\frac{1}{3} s\mu_N \kappa_n B + \frac{1}{4} \bar{m}_n \right) \right. \\ &\quad \left. \left(\bar{m}_n k_{F,s}^n E_F^n + \bar{m}_n^3 \ln \left| \frac{k_{F,s}^n + E_F^n}{\bar{m}_n} \right| \right) \right].\end{aligned}\quad (7)$$

For the neutrons we have introduced

$$\bar{m}_n = m^* - s\mu_N \kappa_n B, \quad (8)$$

where the effective baryon masses are given by

$$m^* = m - \Gamma_\sigma \sigma. \quad (9)$$

The pressure of the system is obtained from the expression

$$P_m = \sum_{b=n,p} \mu_b \rho_b - \varepsilon. \quad (10)$$

The energy spectra for protons are neutrons are given by

$$E_{\nu,s}^p = \sqrt{k_z^2 + \left(\sqrt{m^{*2} + 2\nu q_p B} - s\mu_N \kappa_p B \right)^2} + \Gamma_\omega \omega^0 + \frac{1}{2} \Gamma_\rho \rho^0 + \Sigma_0^R, \quad (11)$$

$$E_s^n = \sqrt{k_z^2 + \left(\sqrt{m^{*2} + k_x^2 + k_y^2} - s\mu_N \kappa_n B \right)^2} + \Gamma_\omega \omega^0 - \frac{1}{2} \Gamma_\rho \rho^0 + \Sigma_0^R, \quad (12)$$

respectively, where $\nu = n + \frac{1}{2} - \text{sign}(q) \frac{s}{2} = 0, 1, 2, \dots$ enumerates the Landau levels of the fermions with electric charge q , the quantum number s is +1 for spin up and -1 for spin down cases, and the rearrangement term is given by

$$\Sigma_0^R = \frac{\partial \Gamma_\omega}{\partial \rho} \rho_b \omega_0 + \frac{\partial \Gamma_\rho}{\partial \rho} \rho_3 \frac{\rho_0}{2} - \frac{\partial \Gamma_\sigma}{\partial \rho} \rho^s \sigma, \quad (13)$$

where $\rho^s = \rho_p^s + \rho_n^s$ and $\rho_b = \rho_p + \rho_n$, with the expressions of the scalar and vector densities for protons and neutrons given by [7]

$$\begin{aligned}\rho_p^s &= \frac{q_p B m^*}{2\pi^2} \sum_{\nu=0}^{\nu_{\max}} \sum_s \frac{\sqrt{m^{*2} + 2\nu q_p B} - s\mu_N \kappa_p B}{\sqrt{m^{*2} + 2\nu q_p B}} \ln \left| \frac{k_{F,\nu,s}^p + E_F^p}{\sqrt{m^{*2} + 2\nu q_p B} - s\mu_N \kappa_p B} \right|, \\ \rho_n^s &= \frac{m^*}{4\pi^2} \sum_s \left[E_F^n k_{F,s}^n - \bar{m}_n^2 \ln \left| \frac{k_{F,s}^n + E_F^n}{\bar{m}_n} \right| \right], \\ \rho_p &= \frac{q_p B}{2\pi^2} \sum_{\nu,s} k_{F,\nu,s}^p, \\ \rho_n &= \frac{1}{2\pi^2} \sum_s \left[\frac{1}{3} (k_{F,s}^n)^3 - \frac{1}{2} s\mu_N \kappa_n B \left(\bar{m}_n k_{F,s}^n + E_F^{n2} \left(\arcsin \left(\frac{\bar{m}_n}{E_F^n} \right) - \frac{\pi}{2} \right) \right) \right]\end{aligned}\quad (14)$$

where $k_{F,\nu,s}^p$ and $k_{F,s}^n$ are the Fermi momenta of protons and neutrons which are related to the Fermi energies E_F^p and E_F^n through

$$\begin{aligned}k_{F,\nu,s}^{p2} &= E_F^{p2} - \left[\sqrt{m^{*2} + 2\nu q_p B} - s\mu_N \kappa_p B \right]^2 \\ k_{F,s}^{n2} &= E_F^{n2} - \bar{m}_n^2.\end{aligned}\quad (15)$$

The chemical potentials of nucleons within TW are given by

$$\begin{aligned}\mu_p &= E_F^p + \Gamma_\omega \omega^0 + \frac{1}{2} \Gamma_\rho \rho^0 + \Sigma_0^R \\ \mu_n &= E_F^n + \Gamma_\omega \omega^0 - \frac{1}{2} \Gamma_\rho \rho^0 + \Sigma_0^R.\end{aligned}\quad (16)$$

For TM1 we have similar expressions with the last term, the rearrangement term, equal to zero.

B. Stability conditions for nuclear matter

At subsaturation densities nuclear matter has a liquid-gas phase transition and homogeneous matter is not stable within a given range of densities. The stability conditions for asymmetric nuclear matter, keeping volume and temperature constant, are obtained from the free energy density \mathcal{F} , imposing that this function is a convex function of the densities ρ_p and ρ_n . For stable homogeneous matter, the symmetric matrix with the elements [25, 26],

$$\mathcal{F}_{ij} = \left(\frac{\partial^2 \mathcal{F}}{\partial \rho_i \partial \rho_j} \right)_T, \quad (17)$$

known as stability matrix, must be positive. This corresponds to imposing that the trace and the determinant of \mathcal{F}_{ij} are positive. In terms of the proton and neutron chemical potentials μ_i , the stability matrix is given by

$$\mathcal{F} = \begin{pmatrix} \frac{\partial \mu_n}{\partial \rho_n} & \frac{\partial \mu_n}{\partial \rho_p} \\ \frac{\partial \mu_p}{\partial \rho_n} & \frac{\partial \mu_p}{\partial \rho_p} \end{pmatrix}, \quad (18)$$

with $\mu_i = \frac{\partial \mathcal{F}}{\partial \rho_i} |_{T, \rho_j \neq i}$.

For nuclear matter, the largest eigenvalue of the stability matrix is always positive and the other becomes negative at subsaturation densities. We define the thermodynamical spinodal at $T=0$ as the curve on the ρ_n, ρ_p plane defined by the points for which the determinant of \mathcal{F}_{ij} is zero; that is, the smallest eigenvalue is zero. Inside the region limited by the thermodynamical spinodal the smallest eigenvalue of \mathcal{F}_{ij} is negative and nuclear matter is unstable [26]. At $T=0$, \mathcal{F} is equal to the energy density defined by Eq. (6). The eigenvalues of the stability matrix are given by

$$\lambda_{\pm} = \frac{1}{2} \left(\text{Tr}(\mathcal{F}) \pm \sqrt{\text{Tr}(\mathcal{F})^2 - 4\text{Det}(\mathcal{F})} \right). \quad (19)$$

The stability condition requires that they are both positive. When one curvature becomes negative the system is thermodynamically unstable and can decrease its free energy by going in the instability direction [26], defined by the direction of the eigenvector associated to the negative eigenvalue. The eigenvectors $\delta \rho_{\pm}$ of the stability matrix are given by

$$\frac{\delta \rho_i^{\pm}}{\delta \rho_j^{\pm}} = \frac{\lambda_{\pm} - \mathcal{F}_{jj}}{\mathcal{F}_{ji}}, \quad i, j = p, n. \quad (20)$$

In the following we study the direction of instability inside the spinodal section for both models considered.

C. Stability conditions for *npe* matter

Stellar matter at low densities is formed by protons, neutrons and electrons in equilibrium with respect to weak interaction processes. Until now we have considered the subsaturation instability region of neutron-proton (*np*) nuclear matter. In this section we investigate the effect of the inclusion of electrons on the stability conditions of nuclear matter when electrons are included. In particular, we will calculate the thermodynamical spinodal sections for *npe* (neutron-proton-electron) neutral matter. Since matter is neutral the proton and electron densities must be equal, i.e. $\rho_p = \rho_e$.

Electrons are included in a minimal way in the system, and are described by the following the Lagrangian density

$$\mathcal{L}_e = \bar{\psi}_e (i\gamma_{\mu} \partial^{\mu} - q_e \gamma_{\mu} A^{\mu} - m_e) \psi_e, \quad (21)$$

where ψ_l are the electron Dirac fields and $m_e = 0.511$ MeV.

Including the electrons, the stability matrix (18) becomes

$$\mathcal{F} = \begin{pmatrix} \frac{\partial \mu_n}{\partial \rho_n} & \frac{\partial \mu_n}{\partial \rho_p} \\ \frac{\partial \mu_p}{\partial \rho_n} & \frac{\partial (\mu_p + \mu_e)}{\partial \rho_p} \end{pmatrix}, \quad (22)$$

and the stability conditions are equivalent to the ones indicated in the previous subsection: the trace and the determinant of \mathcal{F} must be positive.

The electron density is given by

$$\rho_e = \frac{|q_e|B}{2\pi^2} \sum_{\nu,s} k_{F,\nu,s}^e \quad (23)$$

where $k_{F,\nu,s}^e$ is the electron Fermi momentum related to the Fermi energy E_F^e by

$$k_{F,\nu,s}^{e2} = E_F^{e2} - (m_e^2 + 2\nu|q_e|B). \quad (24)$$

For npe neutral matter

$$\mathcal{F} = \epsilon + \epsilon_e$$

where ϵ was defined in (6) and the electron contribution is given by

$$\epsilon_e = \frac{|q_e|B}{4\pi^2} \sum_{\nu,s} \left[k_{F,\nu,s}^l E_F^e + (m_e^2 + 2\nu|q_e|B) \ln \left| \frac{k_{F,\nu,s}^e + E_F^e}{\sqrt{m_e^2 + 2\nu|q_e|B}} \right| \right]. \quad (25)$$

We next discuss np nuclear matter and npe neutral matter. β -equilibrium stellar matter is a particular case of npe neutral matter, with the proton and electron fractions defined by chemical equilibrium conditions, namely

$$\mu_p = \mu_n - \mu_e,$$

with μ_p and μ_n defined in (16) and $\mu_e = E_F^e$.

III. RESULTS AND DISCUSSION

In the present section we first show the dependence of the spinodal section on the magnetic field, both for neutron-proton (np) and neutron-proton-electron (npe) matter. From the crossing of the β -equilibrium EOS of stellar matter with the thermodynamical spinodal we make a prevision of the transition density and transition pressure at the inner edge of the crust of a compact star.

For a zero magnetic field, the direction of instability of nuclear matter gives rise to a distillation effect, corresponding to the formation of droplets of dense matter with low isospin asymmetry in a background of a neutron gas with a small fraction of protons. This effect has been observed experimentally in heavy-ion reactions [11]. Therefore, we also discuss the effect of the magnetic field on the direction of instability, namely in which way it affects the distillation effect.

A. Spinodal section np matter

We will first consider np nuclear matter and determine the instability region limited by the spinodal surface. In Fig. 2 and Fig. 3 we show the spinodal sections obtained making $\lambda_- = 0$, where λ_- was defined in Eq. (19), on the (ρ_p, ρ_n) plane for TM1 and TW and for several values of the magnetic field. We define the magnetic field in units of the critical field $B_e^c = 4.414 \times 10^{13}$ G, so that $B = B^* B_e^c$. For a field with the intensity B_e^c the electron cyclotron energy is equal to the electron mass.

We present the numerical results both not including and including the contribution of the anomalous magnetic moment (AMM). In all figures where both cases are considered we show on the left panel the results without the magnetic field and on the right panel the results including the AMM.

The magnetic field has a strong effect not only on the size, giving rise to larger instability regions, but also on the shape of the instability zones which is not symmetric with respect to the $\rho_p = \rho_n$ line, contrary to np matter for $B = 0$. The increase of the instability region is due to Landau quantization which softens the EOS. For magnetic fields $B^* > 2 \times 10^5$, the protons are totally polarized for all the values of the densities considered and the size of the spinodal zone is larger than the one obtained for $B = 0$. Including AMM decreases the spinodal region with respect to the results without AMM for all the values of the magnetic field considered. This behavior is explained by the extra stiffness that the inclusion of AMM brings into the system due to neutron spin polarization.

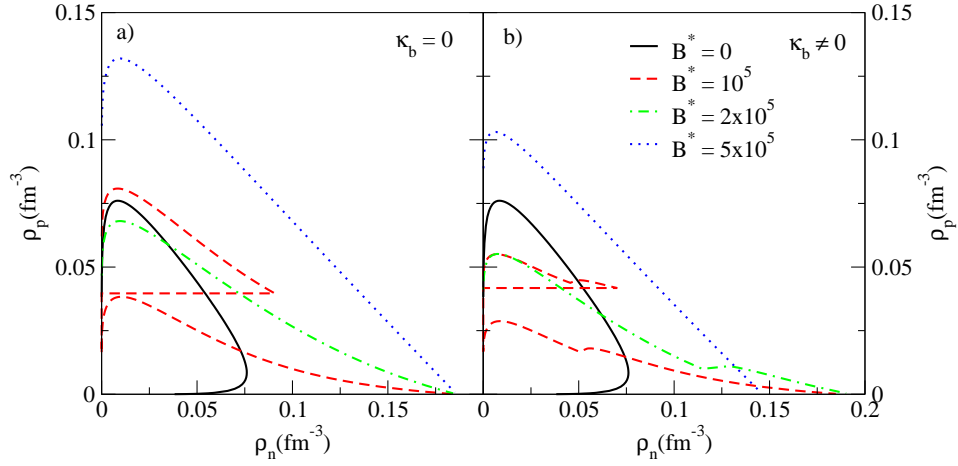


FIG. 2: (Color online) Spinodal section on the ρ_p, ρ_n plane for TM1 at $T = 0$ MeV and for several values of magnetic fields, $B = B^* B_e$, a) without and b) with AMM. For $B^* = 10^5$ the spinodal section is formed by two separate regions.

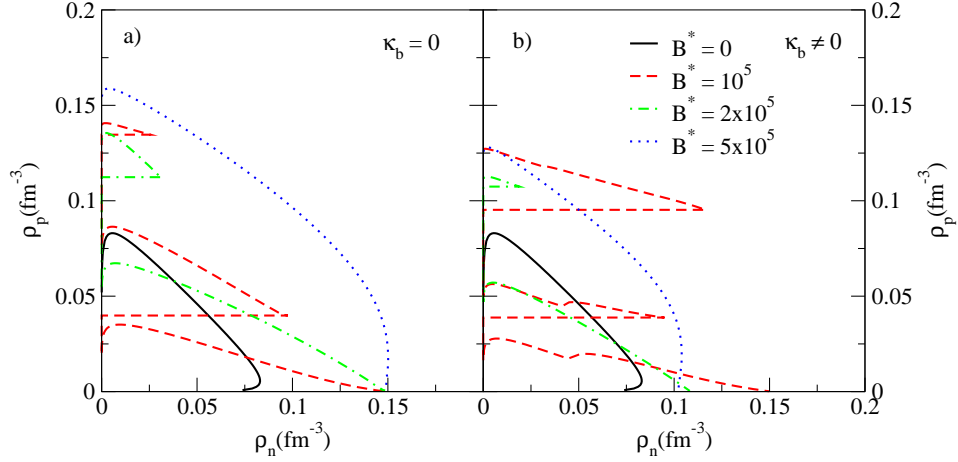


FIG. 3: (Color online) Spinodal section in terms of ρ_p versus ρ_n for TW at $T = 0$ MeV and for several values of magnetic fields a) without and b) with AMM. For $B^* = 10^5$ and 2×10^5 the spinodal section has respectively three and two separated parts.

The effect of the Landau quantization on the spinodal section is explicitly seen in the spinodal for $B^* = 10^5$ for TM1 [dashed line Fig. 2 a)]. The spinodal region consists of two separate zones each one corresponding to one Landau level, the one corresponding to the first Landau level extends to larger neutron densities than the one corresponding to the second level. In order to understand this effect, we plot in Fig. 4 the proton chemical potential for $B^* = 0$, $B^* = 10^5$ and $B^* = 3 \times 10^5$. We have identified the instable regions with thick lines. It is seen that for the larger field the proton chemical potential changes smoothly because for all the densities shown only the first Landau level (LL) is occupied. At low densities the chemical potential decreases with density and only above 0.025 fm^{-3} it starts increasing with density. For $B^* = 10^5$ the proton chemical potential shows a cusp corresponding to the end of the first LL and beginning of the second LL. The unstable regions, in this case, correspond to the beginning of each LL when the slope of the chemical potential is smaller. The smaller the magnetic field the larger the number of LL occupied at subsaturation densities and the larger of independent sections which make up the whole spinodal section. For reference we include the chemical potential at $B = 0$: it increases smoothly with density with a quite constant slope.

If the AMM is included the instabilities regions are smaller, as discussed above. The structure (bump) appearing at $\rho_n \sim 0.05 \text{ fm}^{-3}$ is due to the neutron polarization: below that value of the density the neutrons are totally polarized.

For the TW model with $B^* = 2 \times 10^5$ and 10^5 , Fig. 3, we also get a spinodal region formed by several bands, respectively two and three bands. An interesting feature of this model, is that the band with the largest Landau level may extend to larger neutron densities than lower levels. This does not occur for NLWM and has to do with the behavior of the symmetry energy which increases in a smoother way for DDRHM than for NLWM above $\rho = 0.1 \text{ fm}^{-3}$. As a result the slope of the chemical potentials is not so large.

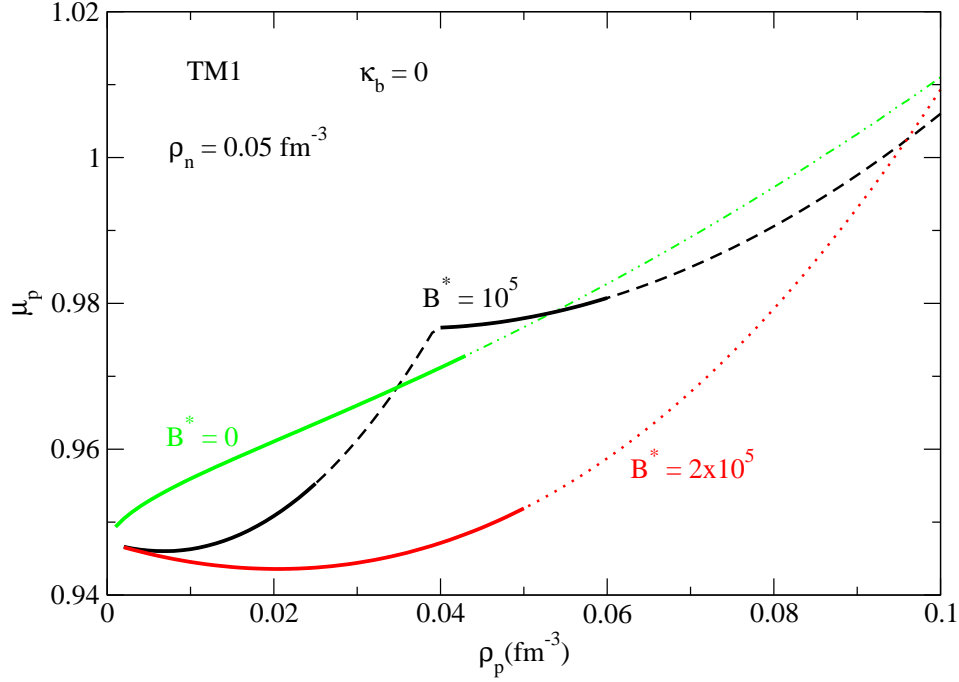


FIG. 4: (Color online) The proton chemical potential for $B = 0$ and for two magnetic field intensities, $B^* = 10^5$ and $B^* = 2 \times 10^5$, obtained within the TM1 model for the neutron density $\rho_n = 0.05 \text{ fm}^{-3}$ and excluding the AMM. The thick lines represent the regions of instability.

Another feature of the spinodal regions with magnetic field and without AMM, that is present in both models we have studied, is the extension of the spinodal for zero proton fraction: in the absence of the magnetic field there is no instability but the inclusion of the magnetic field changes this behavior: the instability region at $\rho_p = 0$ extends until a finite ρ_n value, model dependent, but independent of B . This value is $\sim 0.15 \text{ fm}^{-3}$ for TW and $\sim 0.186 \text{ fm}^{-3}$ for TM1.

To understand this behavior seen at zero proton fraction, we consider the TM1 model. For $\rho_p = 0$, we obtain the corresponding finite value of $\rho_n = \frac{k_F^n{}^3}{3\pi^2}$ from the Fermi neutron momenta k_F^n solution of the equation $\text{Det}(\mathcal{F}) = 0$ with $\rho_p = 0$. Explicitly, the latter equation can be written as follows

$$\left(\mathcal{A}_+ - \frac{\mathcal{C}}{m^{*2}} - \mathcal{D} \right) \left(\frac{\pi^2}{E_F^n k_F^n} + \mathcal{A}_+ - \frac{\mathcal{C}}{E_F^n{}^2} - \mathcal{D} \right) - \left(\mathcal{A}_- - \frac{\mathcal{C}}{m^* E_F^n} - \mathcal{D} \right)^2 = 0 \quad (26)$$

where $\mathcal{A}_\pm = \left(\frac{g_\omega}{m_\omega} \right)^2 \pm \frac{1}{4} \left(\frac{g_\rho}{m_\rho} \right)^2$, $E_F^n = \sqrt{k_F^n{}^2 + m^{*2}}$, and $\mathcal{C} = \left(\frac{g_\sigma}{m_\sigma} \right)^2 \frac{m^{*2}}{\mathcal{K}}$ with,

$$\mathcal{K} = 1 + \left(\frac{g_\sigma}{m_\sigma} \right)^2 \left[2b(g_\sigma \sigma) + 3c(g_\sigma \sigma)^2 + \frac{1}{2\pi^2 E_F^n} \left(k_F^n{}^3 + 3m^{*2} k_F^n - 3m^{*2} E_F^n \log \left| \frac{k_F^n + E_F^n}{m^*} \right| \right) \right] \quad (27)$$

$$\text{and } \mathcal{D} = \frac{\frac{1}{2}\xi \left(\frac{g_\omega}{m_\omega}\right)^4 (g_\omega \omega^0)^2}{1 + \frac{1}{2}\xi \left(\frac{g_\omega}{m_\omega}\right)^2 (g_\omega \omega^0)^2}.$$

This equation is independent of the magnetic field and, therefore, all the spinodal regions for different magnetic fields, without AMM, in Figs. 2 and 3 have the same value of ρ_n for $\rho_p = 0$. The inclusion of AMM changes this feature: ρ_n is still finite for $\rho_p = 0$ but its value is B dependent.

For models with density dependent couplings the spinodal region extends to larger densities for the larger proton densities when compared with NLWM. This is due to the behavior of the symmetry energy: while for NLWM the symmetry energy increases quite steeply for densities above saturation densities, DDRH models have a much smoother behavior and the symmetry energy of these models take much smaller values than NLWM for densities above $\rho = 0.15 \text{ fm}^{-3}$.

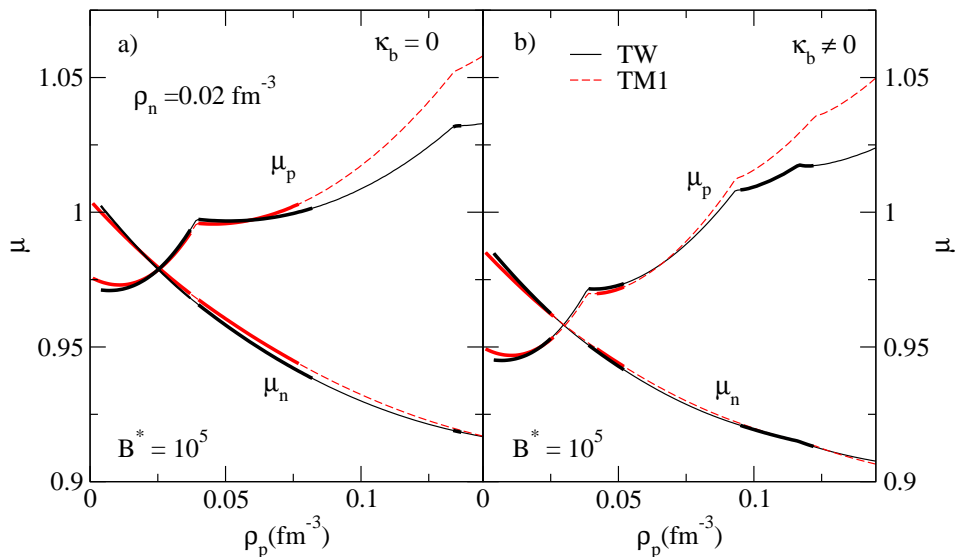


FIG. 5: (Color online) Proton and neutron chemical potentials as function of the proton density for $\rho_n = 0.02 \text{ fm}^{-3}$ and for $B^* = 10^5$ a) without and b) with AMM for TM1 (dashed line) and TW (full line). The thick segments of each curve represent the regions of instability.

In Fig. 5 we plot μ_p and μ_n for $B^* = 10^5$ with the models TM1 (dashed lines) and TW (full lines). The thick segments of the curves lines identify the instability regions defined by the two (TM1) and three (TW) bands which form the spinodal. These curves are obtained for a fixed neutron density, $\rho_n = 0.02 \text{ fm}^{-3}$. It is seen that above $\rho_p = 0.1 \text{ fm}^{-3}$ the proton chemical potential within TW is much softer and this seems to be the reason for the appearance of the third band in this model.

For each model TM1 and TW we identified the crossing density, and corresponding pressure, of the EOS of β -equilibrium stellar matter and the corresponding spinodal for each value of the magnetic field considered. The EOS of state was obtained considering neutrons, protons and electrons in β -equilibrium. In order to illustrate what was done we represent in Fig. 6 the spinodal sections obtained within TM1 for $B^* = 0, 10^5$ and 5×10^5 respectively by full, dashed and dotted thick lines. We include in the same figure, using thin lines with the same type of curve for each B value, the corresponding EOS of β -equilibrium stellar matter. The crossing spinodal-EOS is identified by a big dot. Both the spinodal and the EOS are plotted in the ρ_p, ρ_n plane.

The crossing density of the EOS with the thermodynamical spinodal gives a prevision of the transition density [27, 28] to an homogeneous phase, and is always larger than the one obtained from the crossing of the EOS with the dynamical spinodal for npe matter, which includes the Coulomb interaction. In [29] the authors have shown how the transition density and respective pressure were related to the fraction of the star's moment of inertia contained in the solid crust, and obtained a relation between the radius and mass of compact stars.

In Tables II and III the values of the crossing density and respective pressure are given for stellar matter under different magnetic fields, respectively without and with the AMM. The values of the crossing density for $B = 0, 0.069$

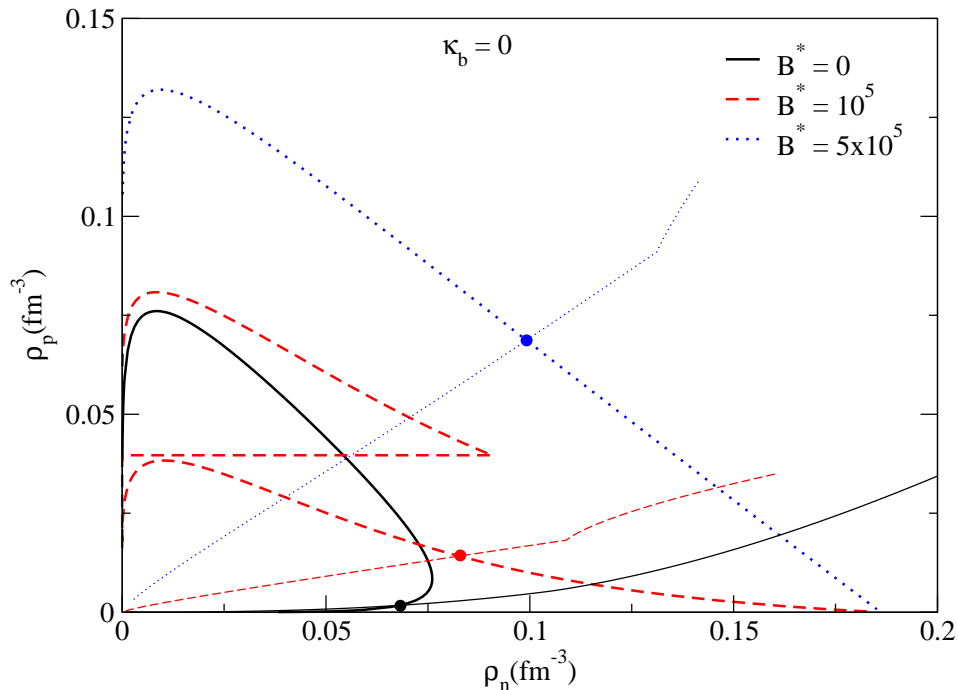


FIG. 6: (Color online) Spinodal section in the ρ_p, ρ_n plane for TM1 at $T = 0$ MeV and for several values of the magnetic field without AMM. For each value of the magnetic field, it also plotted the EOS of stellar matter in β -equilibrium (thin lines). The crossing of the EOS with the respective spinodal, large dot in each spinodal, represent the transition density to continuous matter.

TABLE II: Predicted density, proton fraction and pressure at the inner edge of the crust of a compact star at zero temperature, as defined by the crossing between the thermodynamical instability region of np matter and the β -equilibrium EOS for homogeneous, neutrino-free stellar matter in the ρ_p, ρ_n plane. The AMM is not included.

B^*	Models	$\rho_b^{\text{CROSS}} (\text{fm}^{-3})$	Y_p	$P_m (\text{MeV fm}^{-3})$
0	TM1	0.069509	0.024713	0.50288
	TW	0.084955	0.036690	0.52246
10^5	TM1	0.097030	0.14645	0.95944
	TW	0.10099	0.14641	0.67321
2×10^5	TM1	0.12266	0.24283	1.4008
	TW	0.12786	0.23599	1.0156
3×10^5	TM1	0.14085	0.31304	1.5944
	TW	0.15159	0.30219	1.3795
5×10^5	TM1	0.16783	0.40921	1.6324
	TW	0.19784	0.40194	2.3310

fm^{-3} for TM1 and 0.085 fm^{-3} for TW, can be compared with the corresponding ones obtained from the crossing of the dynamical spinodal with the EOS Ref. [20, 27], respectively 0.06 fm^{-3} for TM1 and 0.075 fm^{-3} for TW. As expected they are a bit larger, with TW model having a larger crossing density than the other. The effect of the magnetic field is to increase the values of the crossing density: at $B^* = 10^5$ both models have similar transition densities of the order of $\sim 0.1 \text{ fm}^{-3}$ corresponding to a much larger pressure for TM1 than TW. For $B^* = 3 \times 10^5$ the transition densities increase to $\rho \sim 0.14 - 0.15 \text{ fm}^{-3}$.

In Table III we show the same data given in Table II but including the AMM in the calculation. The conclusions are similar: the transition density increases with the increase of the magnitude of the magnetic field but not so fast. However, the corresponding pressures are larger than before. We conclude that the existence of a strong magnetic

TABLE III: Predicted density, proton fraction and pressure at the inner edge of the crust of a compact star at zero temperature, as defined by the crossing between the thermodynamical instability region of np matter and the β -equilibrium condition for homogeneous, neutrino-free stellar matter. The case where the AMM is included.

B^*	Models	$\rho_b^{\text{cross}} (\text{fm}^{-3})$	Y_p	$P_m (\text{MeV fm}^{-3})$
10^5	TM1	0.086942	0.17670	1.3801
	TW	0.091391	0.17829	1.2809
2×10^5	TM1	0.096337	0.29468	1.5373
	TW	0.092438	0.30512	1.3549
3×10^5	TM1	0.11046	0.37135	1.7091
	TW	0.11251	0.38035	1.8047
5×10^5	TM1	0.12822	0.47093	1.6616
	TW	0.14880	0.48803	2.7717

field at the crust gives rise to a larger crust.

B. Spinodal section npe matter

We have studied the effect of the magnetic field on the instability region of np matter in the previous section. For npe matter without magnetic field, NLWM models still present a small thermodynamical instability region but for DDRHM models there is no instability region [15]. The incompressibility of the free electron gas is so high that the spinodal disappears or almost disappears.

In Fig. 7 the spinodals for npe matter are shown for TM1 and different magnetic fields. In fact, although including electrons, the instability region can become almost as large as the $B = 0$ np -spinodal. This is due both to the Landau quantization of the orbital motion of protons and electrons: the incompressibility of the electron gas is smaller than the one of a magnetic free electron gas.

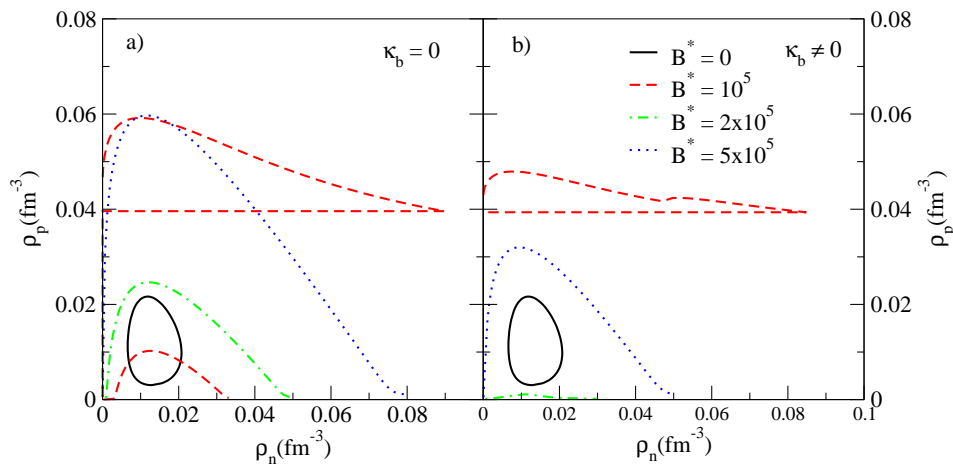


FIG. 7: (Color online) Spinodal section in terms of ρ_p versus ρ_n for TM1 for npe neutral matter at $T = 0$ MeV and for several values of magnetic fields (a) without and (b) with AMM.

For TW, contrary to the $B = 0$ case, the inclusion of the magnetic field gives rise to a spinodal region as seen in Fig. 8. The behavior of this model with the magnetic field is similar to TM1. We also point out that the inclusion of the AMM has a strong effect on the spinodal part corresponding to the first LL: it is drastically reduced or even disappears.

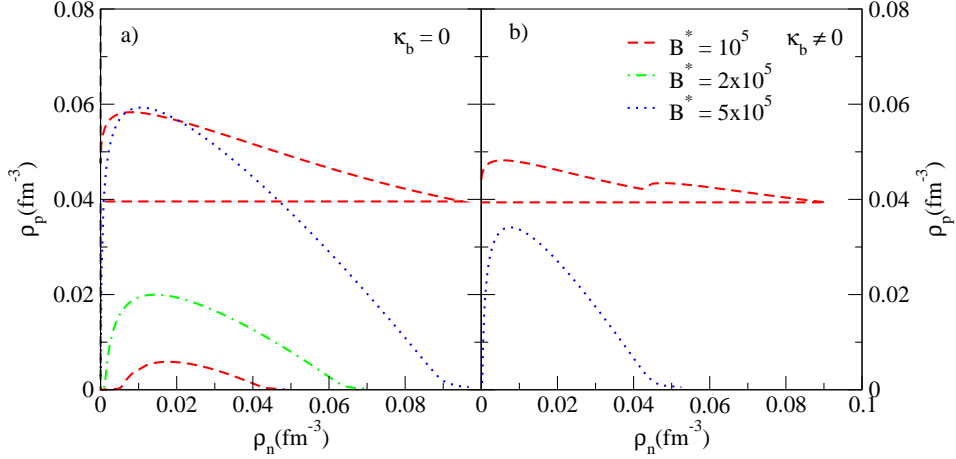


FIG. 8: (Color online) Spinodal section in terms of ρ_p versus ρ_n for TW for npe neutral matter at $T = 0$ MeV and for several values of magnetic fields (a) without and (b) with AMM.

C. Direction of instability

The eigenvector associated with the negative eigenvalue of the free energy curvature matrix defines the direction of the instability and tells us how does the system separate into a dense liquid and a gas phase. It was shown in [15, 20] that in the absence of the magnetic field the direction of instability favors the reduction of the isospin asymmetry of the dense clusters of the system, and increases the isospin asymmetry of the gas surrounding the clusters, the so called distillation effect. This effect is represented in Fig. 9 where it is seen that for the $B = 0$ curve (thick full line) the fraction $\delta\rho_p^-/\delta\rho_n^-$ is larger than ρ_p/ρ_n below $y_p = 0.5$ and the other way round above.

In Fig. 9 we plot, for TM1, the ratio $\delta\rho_p^-/\delta\rho_n^-$ for $\rho = 0.06 \text{ fm}^{-3}$ as a function of the proton fraction. Several results for different values of the magnetic field are shown by the thick lines. The thin lines represent the ratio ρ_p/ρ_n for reference and $y_p = 0.5$ points corresponding to symmetric matter, as well as $\delta\rho_p^-/\delta\rho_n^- = 1$, which is the ratio of density fluctuations for symmetric matter with no field. For the largest field considered the spinodal region contains a single Landau level and the curve varies smoothly starting at $\delta\rho_p^-/\delta\rho_n^- \sim 1.5$. We point out the very large value of this fraction, always above 1, for $y_p < 0.5$. The magnetic field favors an increase of the proton fraction quite above the symmetric matter value. For $B^* = 10^5$ the spinodal has two bands, see Fig. 2 and 3, corresponding to the occupation of the first two Landau levels. The transition from one to the other is clearly seen with a large discontinuity of $\delta\rho_p^-/\delta\rho_n^-$ at $y_p \sim 0.7$. Above this y_p value the curve behaves like the previous ones. However for $y_p < 0.7$ the behavior is quite different: the curve decreases from the value at $y_p = 0$, which is independent of the magnitude of the magnetic field, to a value much smaller than the corresponding value of the fraction ρ_p/ρ_n . The fluctuations will not drive the system out of the first Landau level and therefore the larger the proton fraction, the closer the system comes to the top of the band and the smaller are the allowed proton fluctuations. For $y_p > 0.7$ or for the larger magnetic fields the Landau levels are only partially filled and the fluctuations will never drive the system out of the corresponding Landau level.

Similar features are obtained for TW and/or including the AMM. In Fig. 10 we show, respectively for TM1 (top) and TW (bottom), the fraction $\delta\rho_p^-/\delta\rho_n^-$ as a function of y_p for a fixed baryonic density, $\rho = 0.06 \text{ fm}^{-3}$, chosen inside the instability region. For $y_p > 0.5$, TM1 and TW behave in a similar way, while below this value the main difference is the smaller $\delta\rho_p^-/\delta\rho_n^-$ for TW, corresponding to a smaller distillation effect. This behavior is also present for $B = 0$ and it was shown that this was due to the presence of the rearrangement term. The inclusion of the AMM favors larger proton fractions because neutron polarization stiffens the EOS.

In Figs. 11 and 12 we represent the fraction $\delta\rho_p^-/\delta\rho_n^-$ as a function of density respectively for two values of y_p , 0.2 and 0.4, for np matter (thick lines) and npe matter (thin lines). We consider TM1 and TW. Both models have a very similar behavior for finite values of B although for $y_p = 0.2$ and $B = 0$ they differ: for TM1, $\delta\rho_p^-/\delta\rho_n^-$ increases with density while, for TW, this fraction decreases for $\rho > 0.02 \text{ fm}^{-3}$. This effect is not so strong for $y_p = 0.4$ and for npe matter the fraction is always quite small due to the presence of electrons which prevents large proton variations.

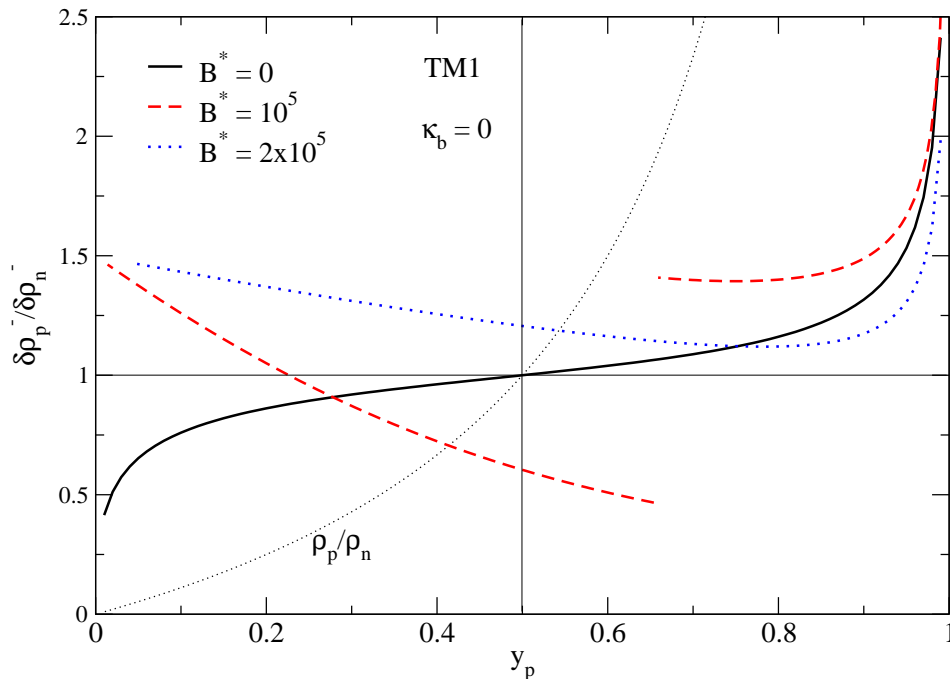


FIG. 9: (Color online) $\delta\rho_p^-/\delta\rho_n^-$ plotted as a function of the proton fraction with $T = 0$ MeV and $\rho = 0.06 \text{ fm}^{-3}$ for the TM1 model and several values of the magnetic fields without AMM. The fraction ρ_p/ρ_n is given by the thin dotted line.

For $B = 10^5$, $\delta\rho_p^-/\delta\rho_n^-$ decreases with density while for $B = 5 \times 10^5$ the opposite occurs. In both cases only the first Landau level is occupied, however for the lower field the first Landau level is almost full and the density fluctuations will occur in such a way that the system stays in the same Landau level: the larger the total density the smaller the fluctuations. For the larger field the first Landau level is only partially filled, far the top of the band. For the same nuclear density, the larger the proton fraction the lower the system energy and therefore the fraction $\delta\rho_p^-/\delta\rho_n^-$ increases with density.

In Fig. 12 we give the same information with $y_p = 0.4$. While for $B^* = 5 \times 10^5$ for the range of densities considered, matter occupies only one Landau level, for $B^* = 10^5$ we may have two (TM1) or three (TW) Landau levels, see Figs. 2 and 3. This explains the discontinuities occurring for $\sim 0.1 \text{ fm}^{-3}$. For the highest magnetic field only one Landau level partially filled comes into play and therefore the fraction $\delta\rho_p^-/\delta\rho_n^-$ increases with density because that is favored energetically. For $B^* = 10^5$ the presence of almost filled Landau levels prevents the existence of large proton density fluctuations.

IV. CONCLUSIONS AND OUTLOOK

In the present work we have studied the instabilities of np matter and npe neutral matter under very strong magnetic fields. The fields considered are much stronger than the strongest field measured until now at the surface of a magnetar which is $B^* \sim 10^2$ for SGR 1806-20 [4]. However, it is expected that fields in the interior of neutrons stars will be much larger. The present work shows how fields of the order of $B = 5 \times 10^{18}$ G could affect the inner crust of a compact star.

We have considered two relativistic nuclear models: one NLW model (TM1) and one DDRH model (TW). For both models, we have determined the spinodal surface, from the curvature matrix of the free energy, for different magnitudes of the magnetic field. It was shown that the instability region could be divided into several bands according to the magnitude of the magnetic field and the number of the Landau levels occupied. The presence of the magnetic field will generally increase the instability region. Making a crude estimation of the transition density at the inner crust of a compact star under a strong magnetic field from the crossing of the EOS of β -equilibrium stellar matter with

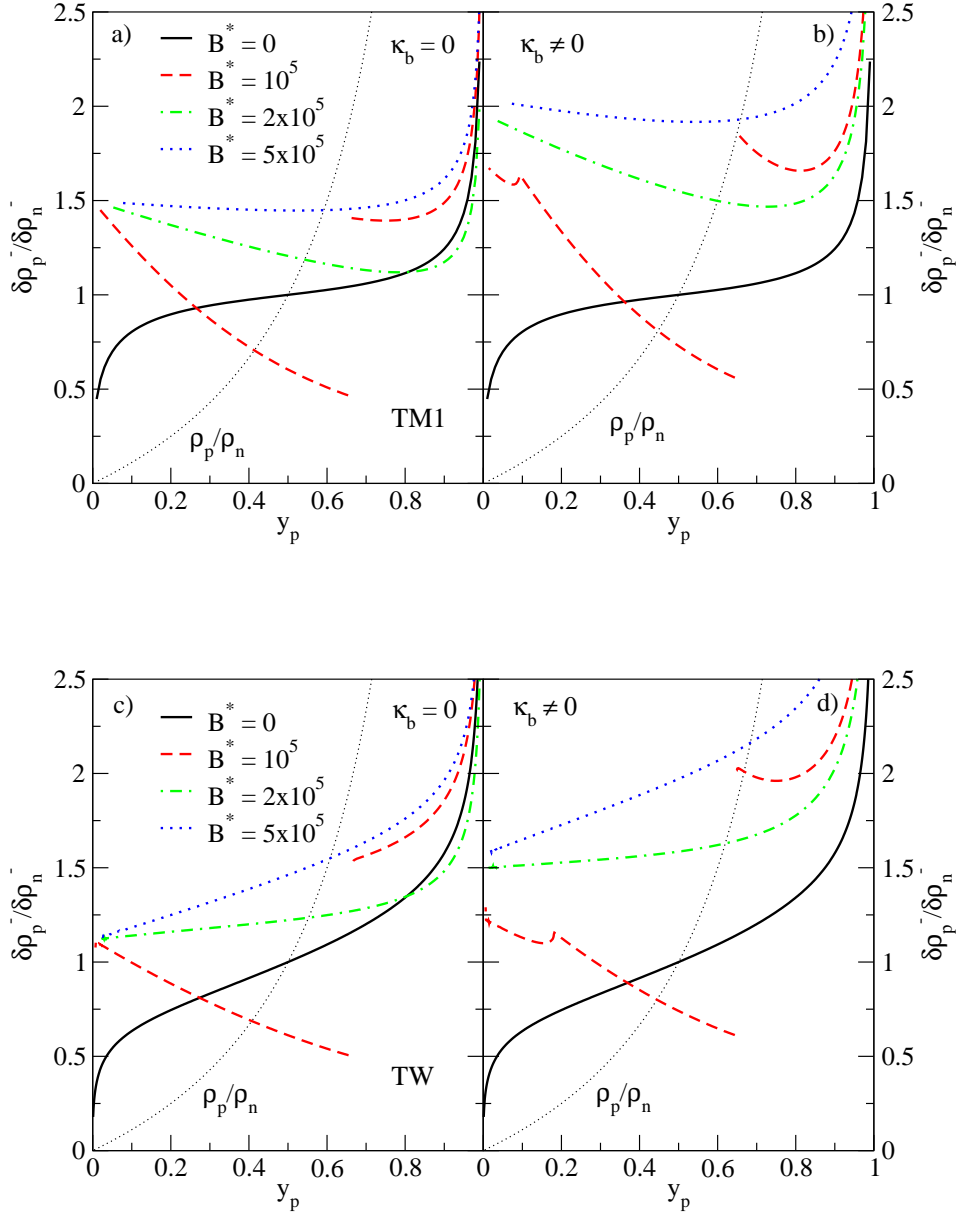


FIG. 10: (Color online) $\delta\rho_p^-/\delta\rho_n^-$ plotted as a function of the proton fraction with $T = 0$ MeV and $\rho = 0.06$ fm $^{-3}$ for the TM1 (top) and TW (bottom) and for several values of the magnetic fields without (a) and (c) and with (b) and (d) AMM. The fraction ρ_p/ρ_n is given by the thin dotted line.

the thermodynamical spinodal, it was shown that the transition density and associated pressure increases with the magnetic field. This will affect the structure of the star increasing the fraction of mass and of the star's moment of inertia concentrated at the crust. These effects will be noticeable if, for densities of the order of 0.1 fm $^{-3}$, the magnetic field is of the order of $B^* = 10^4$ or larger.

The TW model has larger instability regions than the TM1 model for the larger proton densities. A smoother increase of the proton chemical potential for the first model justifies this behavior. This behavior of the symmetry energy may even give rise to a larger number of bands in the spinodal of TW than the spinodal of TM1 for the same magnetic field.

We have also investigated the direction of instability. It was shown that if the Landau level is only partially occupied the density fluctuations are such that the system evolves for a state with dense clusters very proton rich immersed in a proton poor gas. A larger proton fraction is favored energetically due to the degeneracy of the Landau levels. If on the other hand, we study the fluctuation of particles occupying an almost complete Landau level, proton fluctuations cannot be so large and it may even occur an anti-distillation effect with a decrease of the proton fraction of the dense

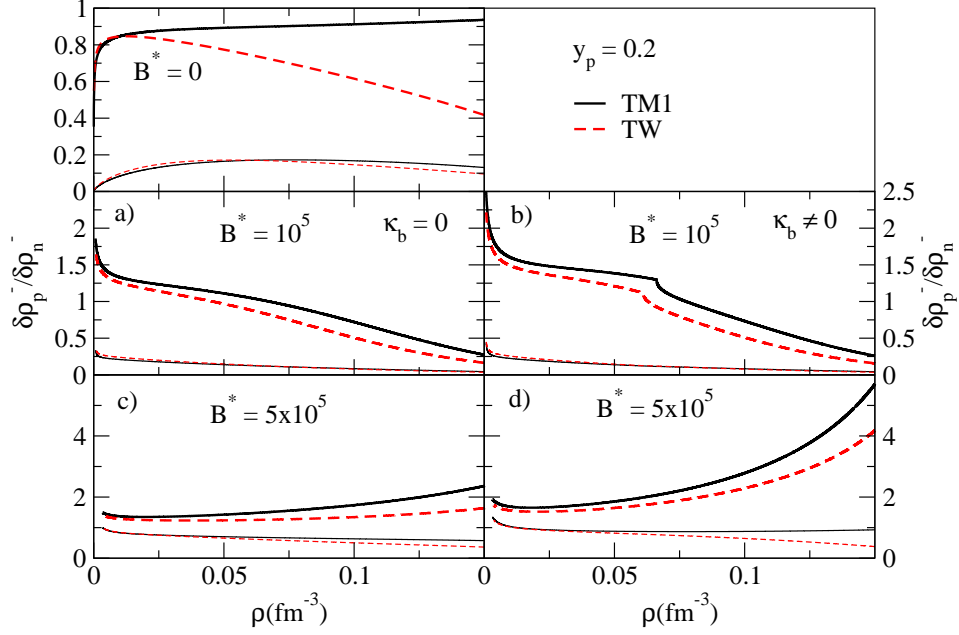


FIG. 11: (Color online) $\delta\rho_p^-/\delta\rho_n^-$ plotted as a function of the density with $T = 0$ MeV and $y_p = 0.2$ with (thin lines) and without (thick lines) electrons for the TM1 and TW models and for several values of the magnetic fields (a) and (c) without and (b) and (d) with AMM.

clusters. This is due to the fact that these fluctuations will keep the system in the same Landau level.

Acknowledgments

This work was partially supported by FEDER and FCT (Portugal) under the grant SFRH/BPD/14831/2003, and projects PTDC/FP/64707/2006 and POCI/FP/81923/2007.

-
- [1] R. C. Duncan and C. Thompson, *Astrophys. J.* 392, L9 (1992); C. Thompson and R. C. Duncan, *MNRAS* 275, 255 (1995).
 - [2] V. V. Usov, *Nature* 357, 472 (1992).
 - [3] B. Paczyński, *Acta Astron.* 42, 145 (1992).
 - [4] SGR/APX online Catalogue, <http://www.physics.mcgill.ca/~pulsar/magnetar/main.html>
 - [5] C. Kouveliotou, S. Dieter, T. Strohmayer, J. van Paradijs, G.J. Fishman, C.A. Meegan, K. Hurley, *Nature* 393, 235 (1998).
 - [6] D. Lai, S.L. Shapiro, *Astrophys. J.* 383, 745 (1991); V. Canuto, J. Ventura, *Fund. Cosmic Phys.* 2, 203 (1977); I. Fushiki, E.H. Gudmundsson, C.J. Pethick, *Astrophys. J.* 342, 958 (1989); A.M. Abrahams, S.L. Shapiro, *Astrophys. J.* 374, 652 (1991); Ö. E. Rögnvaldsson, I. Fushiki, E.H. Gudmundsson, C.J. Pethick, J. Yngvason, *J. Astrophys. J.* 416, 276 (1993).
 - [7] A. Broderick, M. Prakash, and J. M. Lattimer, *Astrophys. J.* 537, 351 (2000).
 - [8] S. Chakrabarty, *Phys. Rev. D* 54, 1306 (1996); S. Chakrabarty, D. Bandyopadhyay, and S. Pal, *Phys. Rev. Lett.* 78, 2898 (1997).
 - [9] B. D. Serot and J.D. Walecka, *Adv. Nucl. Phys.* 16, 1 (1986); J. Boguta and A. R. Bodmer, *Nucl. Phys.* A292, 413 (1977).
 - [10] A. Rabhi, C Providência, and J. da Providência, *J. Phys. G: Nucl. Part. Phys.* 35, 125201 (2008).
 - [11] Ph. Chomaz and F. Gulminelli, *Phys. Lett.* **B447**, 221 (1999); H. S. Xu, *et al*, *Phys. Rev. Lett.* **85**, 716 (2000); Ph. Chomaz, *Nucl. Phys.A* 681, 199c (2001)
 - [12] D. G. Ravenhall, C. J. Pethick, and J. R. Wilson, *Phys. Rev. Lett.* 50, 2066 (1983)
 - [13] C. J. Horowitz, M. A. Perez-Garcia, and J. Piekarewicz, *Phys. Rev. C* 69 045804(2004).
 - [14] Y. Mochizuki and T. Izuyama, *Astrophys. J.* 440, 263 (1995)
 - [15] S. S. Avancini, L. Brito, Ph. Chomaz, D. P. Menezes, and C. Providência, *Phys. Rev. C* 74, 024317 (2006).

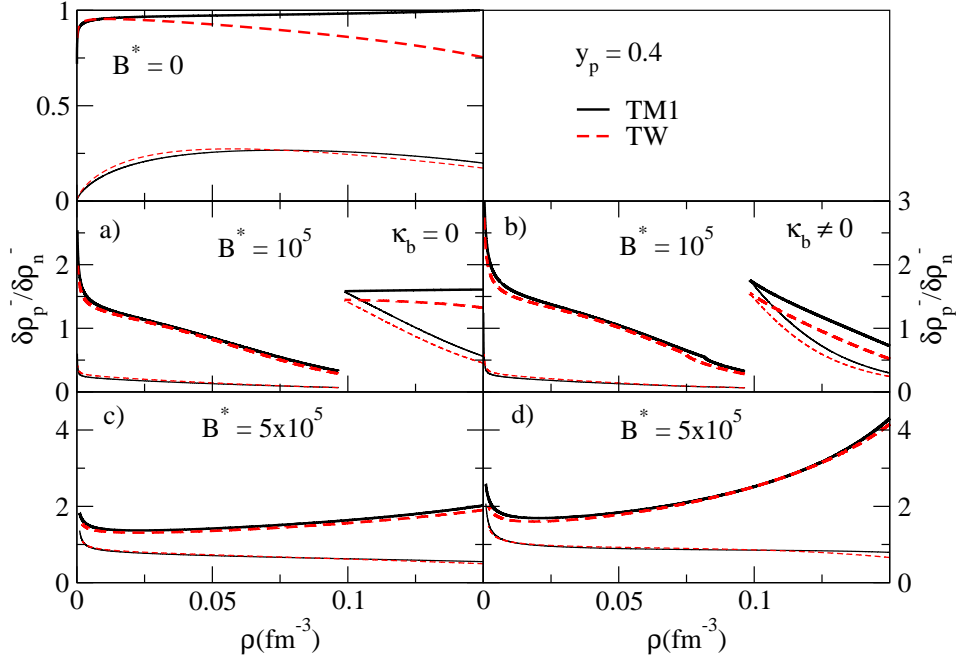


FIG. 12: (Color online) $\delta\rho_p^-/\delta\rho_n^-$ plotted as a function of the density with $T = 0$ MeV and $y_p = 0.4$ with (thin lines) and without (thick lines) electrons for the TM1 and TW models and for several values of the magnetic fields a) without and b) with AMM.

- [16] C. Providência, L. Brito, S.S. Avancini, D. P. Menezes and Ph. Chomaz, Phys. Rev. C 73, 025805 (2006).
- [17] Deborah N. Aguilera, José A. Pons, Juan A. Miralles, astro-ph/0710.0854
- [18] Y. Sugahara and H. Toki, Prog. Theor. Phys. 92, 803 (1994).
- [19] S. Typel and H. H. Wolter, Nucl. Phys. A656, 331 (1999).
- [20] Camille Ducoin, Constança Providência, Alexandre M. Santos, Lucilia Brito, Philippe Chomaz, arXiv:0808.0233
- [21] C. Fuchs, H. Lenske, and H. H. Wolter, Phys. Rev. C 52, 3043 (1995).
- [22] R. Brockmann and R. Machleidt, Phys. Rev. C 42, 1965 (1990); S. Haddad and M. K. Weigel, Phys. Rev. C 48, 2740 (1993); F. de Jong and H. Lenske, Phys. Rev. C 57, 3099 (1998).
- [23] G. Hua, L. Bo, and M. Di Toro, Phys. Rev. C 62, 035203 (2000).
- [24] Y. F. Yuan and J. L. Zhang, ApJ, 525, 950, (1999); G.-J. Mao, A. Iwamoto and Z.-X. Li, Chin. J. Astron. Astrophys. Vol.3, No 4, 359-374 (2003)
- [25] H. Müller and B. D. Serot, Phys. Rev. C 52, 2072 (1995) V. Baran, M. Colonna, M. Di Toro, and A. B. Larionov, Nucl. Phys. A632, 287 (1998).
- [26] J. Margueron and P. Chomaz, Phys. Rev. C 67, 041602(R) (2003).
- [27] S.S. Avancini, D.P. Menezes, M.D. Alloy, J.R. Marinelli, M.M.W. Moraes and C. Providência, Phys. Rev. C 78, 015802 (2008).
- [28] J. Xu, L.W. Chen, B.A. Li and H.R. Ma, arXiv:0807.4477v1 [nucl-th].
- [29] Bennett Link, Richard I. Epstein, and James M. Lattimer, Phys. Rev. Lett. 83, 3362 (1999).
- [30] A. M. Santos, L. Brito, and C. Providência, Phys. Rev. C 77, 045805 (2008).